Received: 30 November 2022 | Accepted: 3 February 2023

DOI: 10.1002/pip.3680

RESEARCH ARTICLE

PROGRESS IN PHOTOVOLTAICS WILEY

TOPCon shingle solar cells: Thermal laser separation and passivated edge technology

Elmar Lohmüller[1] | Puzant Baliozian[1,2] | Leon Gutmann[1] | Leander Kniffki[1] | Armin Richter[1] | Lili Wang[3] | Ricky Dunbar[3] | Arnaud Lepert[3] | Jonas D. Huyeng[1] | Ralf Preu[1]

[1]Fraunhofer Institute for Solar Energy Systems ISE, Heidenhofstraße 2, Freiburg, 79110, Germany

[2]now with VDMA Photovoltaic Equipment, Lyoner Str. 18, Frankfurt am Main, 60528, Germany

[3]The Solaria Corporation, 45700 Northport Loop E, Fremont, CA, 94538, USA

Correspondence
Elmar Lohmüller, Fraunhofer Institute for Solar Energy Systems ISE, Heidenhofstraße 2, 79110 Freiburg, Germany.
Email: elmar.lohmueller@ise.fraunhofer.de

Funding information
German Federal Ministry for Economic Affairs and Climate Action, Grant/Award Number: 03EE1101A; Solaria Corporation

Abstract

This work shows the first demonstration of thermal laser separation (TLS) and post-metallization passivated edge technology (PET) applied to tunnel-oxide passivated contact (TOPCon) shingle solar cells. The shingle solar cells with 26.46 mm × 158.75 mm size are separated from industrial full-square TOPCon host solar cells. The singulation is performed either by TLS from the front side (emitter side) or by conventional laser scribe and mechanical cleaving (LSMC) from the rear side (emitter-free side). The TLS optimized in this work yields up to 0.2%$_{abs}$ more efficient shingle cells after separation in comparison with LSMC-separated shingle cells. The most promising PET sequence identified for the singulated TOPCon cells consists of depositing an 8-nm-thin aluminum oxide layer by thermal atomic layer deposition at a temperature below 200°C in conjunction with subsequent hotplate annealing at 250°C. Application of the PET yields a boost of up to 0.5%$_{abs}$ in energy conversion efficiency for edge-passivated TOPCon shingle cells in comparison with their performance directly after separation. This efficiency-increasing impact of the PET sequence is found not to be strongly dependent on the separation process applied. The most efficient TOPCon shingle cell after PET achieves an efficiency of 22.0% and has been singulated by TLS.

KEYWORDS
edge passivation, passivated edge technology, shingle solar cells, surface passivation, thermal laser separation, TOPCon

1 | INTRODUCTION

Cutting large-area solar cells in at least two sub-cells is nowadays very common in the solar cell industry.[1,2] Separated cells result in lower current per cell and a quicker increase of module voltage in series interconnection. In addition to the approach of cutting a large cell into, for example, two or three sub-cells, there is also the approach of singulating even more sub-cells, also known as shingle solar cells.[3,4] Research activities on shingle solar cells were and are being carried out for various solar cell types as for, for example, passivated emitter and rear cells (PERC),[4–8] silicon heterojunction (SHJ) cells,[9–13] or tunnel-oxide passivated contact (TOPCon) cells.[13] SHJ and TOPCon solar cells implement passivating contacts, resulting in increased voltages and higher efficiencies compared with PERC, which is still the

standard in industry today.[14] The amorphous silicon-based SHJ solar cells are usually processed at temperatures of up to around 200°C to maintain their advantages,[15,16] whereas the polycrystalline silicon-based contacts of TOPCon solar cells can withstand similar high-temperature processing as for PERC solar cells. This makes them compatible with existing mass fabrication and of high interest in research and industry.

Surface recombination in solar cells reduces the number of excited charge carriers on all surfaces (leading to power loss) but is more pronounced at newly created, that is, unpassivated, edge surfaces of cut solar cells. As the perimeter-to-area ratio increases with decreasing sub-cell size, edge recombination becomes more and more important the smaller the cells get.[17,18] The impact of edge recombination becomes even more significant with cells of higher efficiency potential. Although edge recombination is also present in today's half- or third-cells, it is of extraordinary importance for shingle cells. Thus, for fabrication of highly efficient shingle cells/modules, the challenge consists in minimizing edge recombination:

i. The cutting of the cells should be performed with low-damage technologies. The reference separation technology is a conventional laser scribe and mechanical cleaving (LSMC) process. To create the breaking point for LSMC, a laser is used to form a continuous scribe (i.e., laser ablation) over the entire length of the silicon cell at the desired positions. This scribe then enables the mechanical cleave into sub-cells. In contrast to LSMC, thermal laser separation (TLS)[19] needs only a very short initial laser scribe to create a starting crack that can then be propagated through the wafer in any direction by a cleave laser combined with a water–air aerosol jet. This results in cuts with very smooth edge surfaces. Several publications have shown application of TLS on PERC[7,20–22] or SHJ[10,21,23] devices. Although it is also applicable to TOPCon solar cells, the authors are not aware of any publication on this.
ii. The charge carrier recombination at the newly created edge surfaces should be minimized. This can be achieved by, for example, edge passivation.[17,24,25] After successful experimental proof of an approach for edge passivation and modeling of the respective potential,[18] Fraunhofer ISE filed a patent application in 2018. In 2019, Fraunhofer ISE introduced the post-metallization passivated edge technology (PET) and demonstrated edge passivation on PERC shingle cells.[7,26] The PET consists of the deposition of a passivation layer after cell separation, for example, an aluminum oxide (Al_2O_3) layer—which is known for excellent passivation quality[27]—with subsequent activation of the same by means of elevated temperature exposure, also referred to as annealing. The temperatures for both processes can be kept at or below 250°C and thus make the PET concept also very attractive for SHJ and TOPCon cells. For SHJ, the PET has been also demonstrated on half-cut cells,[23] and the concept of the PET approach was taken up by INES in 2020[10] and demonstrated on SHJ shingle cells.[10–12,28]

To the authors' knowledge, the application of the PET has so far not been examined for TOPCon shingle cells in already published work. Hence, this paper demonstrates its applicability in conjunction with TLS for TOPCon cell cutting.

2 | APPROACH AND EXPERIMENT

This study aims to develop improved processes for cell separation and edge passivation that can be applied for fabricating high-quality TOPCon shingle solar cells. Conventional LSMC serves as a reference process for cutting silicon cells. We compare this reference process with TLS and optimize the latter for the TOPCon cell architecture. TLS is performed with a "*microDICE*" tool made by *3D-Micromac*.[29] We then proceed to optimize edge passivation for TOPCon shingle solar cells. Finally, the optimized PET sequence is examined on shingle solar cells that have been separated either by LSMC or by TLS.

2.1 | TOPCon host solar cells

The experiment is performed using industrial TOPCon host solar cells. The devices, shown in Figure 1, have front-side boron emitters and are metalized with a six-shingle, bifacial screen-printing design. The host cell has a 158.75-mm edge length (full-square, 223 mm diagonal),

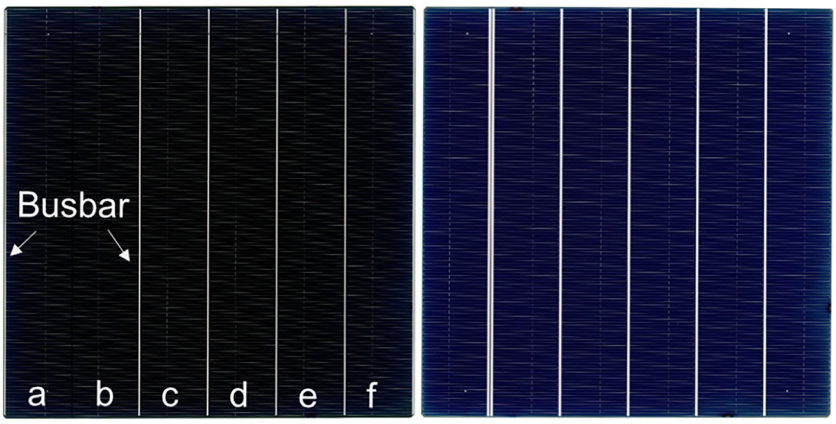

FIGURE 1 Photographs of a tunnel-oxide passivated contact (TOPCon) host cell taken from (left) front side and (right) rear side. The host cell contains six shingle cells marked by the letters a to f with one busbar contact on each cell side. After separation, each shingle cell has a cell size of 26.46 mm × 158.75 mm.

and each shingle solar cell has a final width of 26.46 mm. The continuous front and rear side busbars feature a width of 0.5 and 1 mm, respectively.

2.2 | Experiment plan

The experiment plan is schematically illustrated in Figure 2. It contains three sub-experiments denoted as experiments A to C:

- Experiment A targets the optimization of the TLS process for low-damage cutting of the TOPCon host cells into shingle cells.
- Experiment B targets the optimization of the thermal atomic layer deposition (ALD) of Al_2O_3 for edge passivation.
- Experiment C compares LSMC and TLS as separation techniques applying the findings from experiments A and B.

All TOPCon host cells were selected from the same efficiency bin from one production run. Current–voltage (*I*–*V*) measurements are performed in an automated cell tester using a monofacial setup on black foil and GridTouch[30] contacting. Thirty wires are utilized on each side (front and rear) aligned perpendicular to the busbars and thus parallel to the finger contacts. Some of the host cells are also characterized via SunsV_{OC} measurements.

All shingle cells are measured on the same automated cell tester as has been used for the host cell measurements. The *I*–*V* measurements are also performed in a monofacial setup, that is, without rear side illumination according to the bifacial cells standard *IEC TS 60904-1-2:2019-01*. Unlike the GridTouch contacting scheme used for the host cells, shingle cells are contacted along the busbars on the front and rear sides with pin contact bars. An additional bar is used on both the front and rear on the non-busbar edge for mechanical fixation (i.e., no electrical contacting).

2.2.1 | Experiment A: TLS optimization

The starting point for optimizing the TLS process is the process previously used at Fraunhofer ISE for completely internally fabricated TOPCon shingle solar cells. Based on previous experience, it is a good idea to optimize the TLS process with regard to the host cells actually used. This optimization is performed in three steps:

(A-I) Optimization of the cleave step to minimize/prevent surface damage close to the dividing line.Therefore, different cleave processes are applied either on the front side (emitter side) or on the rear side (emitter-free side) of host cells without initial scribes (i.e., the samples are not cut). This allows an assessment of the cleave step using photoluminescence (PL) imaging as described in Baliozian et al.[21]: Signal drops in the PL intensity after the cleave process indicate a detrimental impact on the surface passivation quality.

(A-II) Ensuring that the optimized cleave process from (A-I) allows the separation of the host cells when the initial scribe is performed.

(A-III) *I*–*V* measurements of shingle solar cells cut either from the front or the rear side by the optimized TLS process resulting from (A-I) and (A-II).

2.2.2 | Experiment B: ALD optimization Al_2O_3 layer

For the optimization of the thermal ALD of Al_2O_3 on shingle cells, the optimized TLS process from Section 2.2.1 is applied from the front side. The ALD process is performed in a "*FlexAl*" system from *Oxford Instruments* using trimethylaluminum and water vapor as precursors. The size of the process chamber allows to process up to 48 shingle cells in one run, where the shingle cells are stacked in four stacks of 12 cells each. Each stack is covered with one dummy shingle cell and

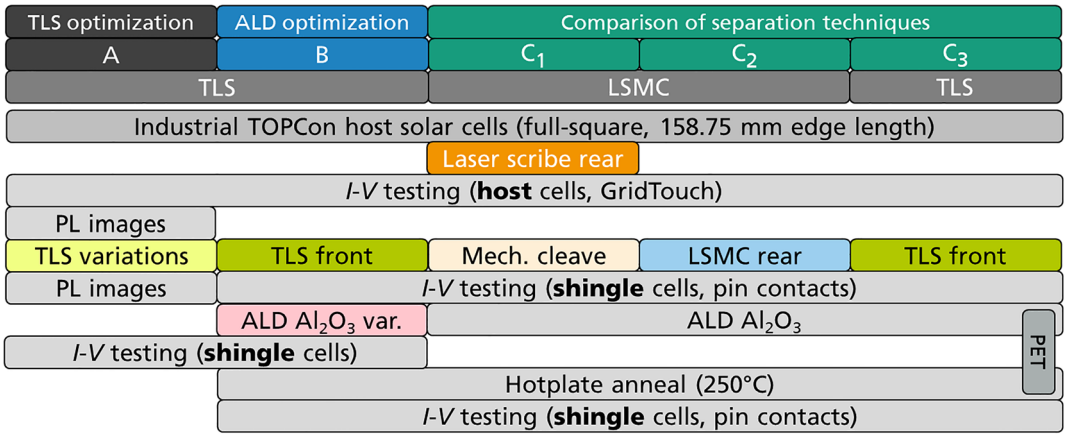

FIGURE 2 Schematic process sequence of the three experiments A, B, and C regarding cell separation and edge passivation for tunnel-oxide passivated contact (TOPCon) shingle solar cells.

a 1-mm-thick piece of glass for weighing down the shingle cell stack so that the cells lie close on top of each other.

Four different ALD processes are examined: all combinations of two Al_2O_3 layer thicknesses of about 8 nm (74 cycles) and about 14 nm (130 cycles) and two different deposition temperatures $T_1 < T_2$, both below 200°C. These deposition temperatures are compatible with the subsequent annealing step performed on a hotplate at a temperature of 250°C. In addition to these four variations, a fifth variation omits the ALD Al_2O_3 layer deposition and tests the impact of the annealing process alone on the shingle cell properties.

2.2.3 | Experiment C: Comparison of separation techniques

For the first two groups C_1 and C_2, two different LSMC processes are trialed with laser scribing on the rear side to cut each host cell into six shingle cells. For group C_1, the laser scribe has been applied without cleaving the samples prior to *I*–*V* testing. This means that the host cells are still in one piece during *I*–*V* testing but feature five continuous laser scribes on the rear side. For group C_3, the optimized TLS process from Section 2.2.1 is applied from the front side to cut each host cell into the six shingle cells.

After the singulation, the *I*–*V* measurements of the shingle cells are performed. SunsV_{OC} measurements are also performed for shingle cells for which the host cell has also been measured by SunsV_{OC}. To compare the SunsV_{OC} results one to one between the host cell and the shingle cell state, the shingle cells are measured with the same contacting scheme at the same location on the SunsV_{OC} chuck as applied for the host cell.[7]

Based on the results from Section 2.2.2, the most promising PET process sequence is applied for edge passivation of the TOPCon shingle cells.

3 | RESULTS AND DISCUSSION

3.1 | Experiment A: TLS optimization

The TOPCon host cells are only exposed to the cleave step within the TLS sequence either on the front or the rear side without initial laser scribing. With the host cells still in one piece, potential damage of their surface passivation due to the cleave process can be quantified and minimized.

Exemplary PL images before and after laser cleaving with two different laser powers are shown in Figure 3. The PL images before the cleave step show a bright area between the shingle cells a and b as there are no busbar contacts present on the front side. After performing the cleave process with higher laser power, this area between a and b is no longer bright but dark. This indicates a degradation of the passivation quality in the area where the spatially extended laser beam of the cleave step interacts with the surface passivation. In contrast, for the lower laser power, the PL images before and after laser cleave are identical. Thus, the PL intensity is not lowered by the cleave step meaning that the surface passivation quality is not impacted.

By applying the initial scribe on further host cells, a successful mechanical separation into shingle cells results for all variations of the cleave process that have been carried out. It is found that the separation from the front side is very robust in comparison with that from the rear side. The *I*–*V* measurements of the shingle cells that are TLS-separated with the optimized laser cleave from the front and rear side (not shown) reveal that the separation from the front side results in almost the same cell performance even though the separation is performed on the side with the emitter present.

In summary, it turns out that an optimized laser cleave process allows the TLS of TOPCon host cells into TOPCon shingle cells without decreasing the surface passivation quality in the vicinity of the cutting channel. In other words, losses observed after TLS can be attributed to edge recombination of the newly created edge surfaces and not to detrimental impact of the TLS process itself.

3.2 | Experiment B: ALD optimization Al_2O_3 layer

The used TOPCon host cells have a mean conversion efficiency $\eta_{mean} = (21.84 \pm 0.05)\%$. *I*–*V* data for the TOPCon host and shingle cells are shown in Figure 4A,B, respectively, grouped by the ALD Al_2O_3 passivation treatment.

Cutting the host cells by TLS into shingle cells leads to losses in open-circuit voltage V_{OC} of $\Delta V_{OC} = -4$ mV and in pseudo fill factor *pFF* of $\Delta pFF = -1.2\%_{abs}$ (on average for all five groups). A clear improvement is then seen in Figure 4B for the first four groups after deposition of the ALD Al_2O_3 layer (blue vs. orange, on average):

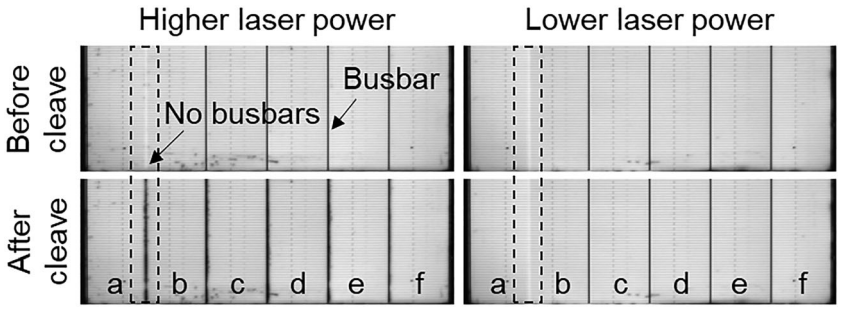

FIGURE 3 Cutouts from photoluminescence (PL) images of a lower part of the host cells (see Figure 1) taken before and after the cleave process on the front side with higher and lower laser power. The cleave process has been applied for all five dividing lines. The results of this test are easiest to see between the two shingle cells a and b (region marked with dashed lines) because of the lack of front side busbar contacts.

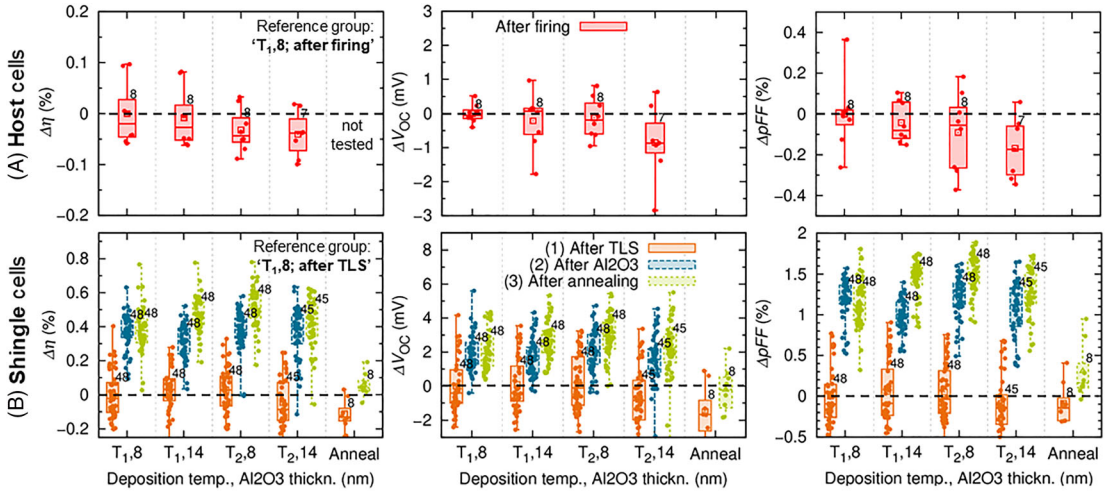

FIGURE 4 *I–V* data from experiment B for the tunnel-oxide passivated contact (TOPCon) (A) host cells and (B) shingle cells, expressed as an absolute offset from the mean of the respective reference group stated. The designation of the first four groups consists of the deposition temperature used and the Al_2O_3 layer thickness in nm. Group "T_1,8," for example, was passivated with deposition temperature T_1 and an Al_2O_3 layer thickness of 8 nm. The small number next to the data points gives the total number of samples per group.

TABLE 1 *I–V* data for the most efficient TOPCon shingle cell from position c (see Figure 1) in different processing states, expressed in each case as an absolute offset from its host cell *I–V* data.

Cell type	State	$\Delta\eta$ (%)	ΔV_{OC} (mV)	ΔpFF (%)
Shingle	(1) After TLS	−0.6	−4	−1.2
	(2) After Al_2O_3 ("T_2,8")	−0.1	−2	+0.2
	(3) After annealing	+0.1	−1	+0.5

Note: The efficiency of the host cell is $\eta = 21.9\%$, and the efficiency of the shingle cell after annealing is $\eta = 22.0\%$.
Abbreviation: TLS, thermal laser separation.

$\Delta V_{OC} = +2$ mV and $\Delta pFF = +1.1\%_{abs}$. The subsequent annealing step further improves the cell parameters for three of the four groups (not for the first group "T_1,8") and yields $\Delta V_{OC} = +3$ mV and $\Delta pFF = +1.3\%_{abs}$ compared with the values measured after TLS (green vs. orange). The ALD process "T_2,8" shows the largest mean gains after annealing ($\Delta\eta = +0.5\%_{abs}$, $\Delta V_{OC} = +3$ mV, and $\Delta pFF = +1.5\%_{abs}$) and thus has been chosen to be applied for edge passivation within experiment C. The metal contacts of the shingle cells are hardly affected by the applied thermal budgets from the ALD of Al_2O_3 and the annealing step, as the cell series resistances R_S are quite stable (not shown).

The evolution of some cell parameters in the different processing states of the most efficient TOPCon shingle cell—with an efficiency $\eta = 22.0\%$ after annealing—are summarized in Table 1 in relation to the data for its host cell. This shingle cell has been processed with the "T_2,8" ALD Al_2O_3 passivation recipe, and it was located within the host cell at position c. This means that this shingle cell features two cut edge surfaces.

It seems that cutting the host cells into shingle cells and applying the PET enables to even achieve larger *pFF* values for the edge-passivated shingle cells than for the host cells. One potential explanation for this observation can be that, in addition to the newly applied surface passivation on the cut edges, the already existing surface passivation in the cell area is also improved by the PET process steps. As is seen for the fifth group "Anneal" in Figure 4B, which has only been annealed (i.e., no Al_2O_3 layer deposition), this temperature treatment itself leads to a quite remarkable improvement in the cell properties with $\Delta\eta = +0.2\%_{abs}$, $\Delta V_{OC} = +1$ mV, and $\Delta pFF = +0.4\%_{abs}$. Apart from natively grown silicon dioxide on the cut edge surfaces, further silicon dioxide could grow during the hotplate anneal leading to some edge passivation. On the other hand, Al_2O_3 layers are well known for having a high hydrogen content.[31] Hydrogen, on the other hand, is known to play an important role in the passivation of silicon surfaces.[32] Our current hypothesis for explaining the partly larger *pFF* values in the shingle cell state compared with those in the host cell state is that the PET sequence slightly improves the surface passivation of the host cells. Further work (e.g., host cell *I–V* testing after ALD of Al_2O_3 or after annealing) would need to be performed to test this hypothesis.

Nevertheless, ALD of Al_2O_3 and annealing has an irrefutable strong positive effect on the shingle cell properties. This makes the PET sequence very promising for highly efficient TOPCon shingle solar cells with passivated edges.

For a selection of shingle cells from the first four groups, also several SunsV_{OC} measurements are performed to examine the stability of the improvement due to the applied PET sequence over time; see Figure 5. In between the SunsV_{OC} measurements, these shingle cells have been stored in ambient condition in the dark. The V_{OC} varies less than 1 mV in the mean values for all four groups and test times and thus can be considered stable within the measurement accuracy. For the *pFF* values, a trend toward slightly decreasing values is seen over time. Although the shingle cells with the Al_2O_3 ALD process "T_1,8" show a mean *pFF* loss of $-0.3\%_{abs}$ after 11 months, process "T_2,8"—which has been chosen for experiment C—results in a mean *pFF* decrease of less than $-0.1\%_{abs}$ during the same period. For the processes "T_1,14" and "T_2,14," the mean *pFF* decrease accounts to $-0.1\%_{abs}$ and $-0.2\%_{abs}$, respectively. Thus, the ALD process for forming the Al_2O_3 passivation layer influences not only the absolute performance of the shingle cells but also their long-term stability. Process "T_2,8" yields extremely promising PET long-term stability data.

3.3 | Experiment C: Comparison of separation techniques

As in the previous section, the *I*–*V* data for the TOPCon host and shingle cells are again shown relative to the specified reference groups in Figure 6A,B, respectively. The shingle cells in groups C_1 and C_2 have been separated by two different LSMC processes from the rear side. The shingle cells in group C_3 have been separated from the front side using the previously optimized TLS sequence. The used TOPCon host cells in group C_3 have $\eta_{mean} = (22.0 \pm 0.05)\%$. As the laser scribes for the host cells from group C_1 have been performed prior to cell testing, the *I*–*V* data already include the associated scribe losses. Furthermore, the data for the shingle cells singulated by the different separation approaches (see Figure 2) are split for each group according to their number of new edges: The "outer" shingle cells at positions a and f within the host cell (see Figure 1) have one new edge surface, and the "inner" shingle cells at positions b to e have two new

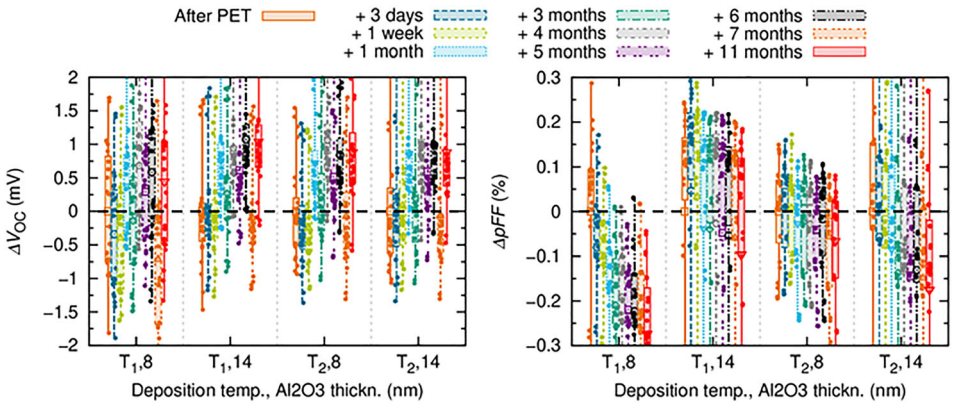

FIGURE 5 SunsV_{OC} data at various times after passivated edge technology (PET) for six tunnel-oxide passivated contact (TOPCon) shingle cells from each of the four different groups in experiment B (each cell has been measured two times at two certain positions). The data are shown as an absolute offset from the mean of each reference group "After PET."

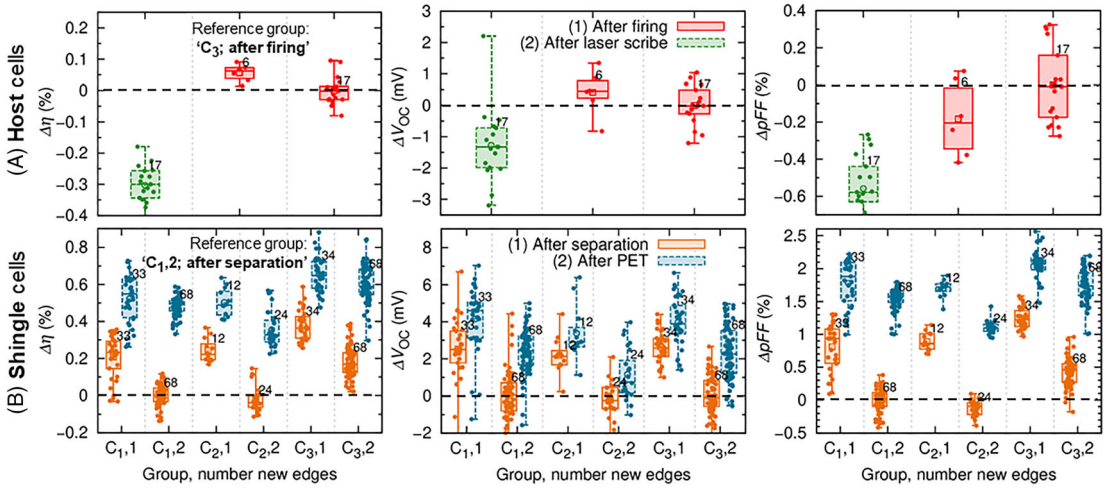

FIGURE 6 *I*–*V* data from experiment C for the tunnel-oxide passivated contact (TOPCon) (A) host cells and (B) shingle cells, expressed as an absolute offset from the mean of the respective reference group stated. For the host cells in group C_1, the laser scribes have been already performed prior to cell testing. The labeling of the *x*-axis for the shingle cells consists of the group C_X ($_X = \{1,2,3\}$) and the number of new edges (1 or 2).

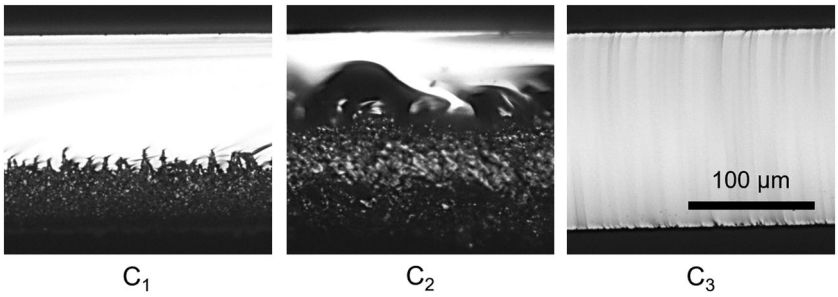

FIGURE 7 Light-microscope images of the edge surface after separation for the three investigated separation approaches. For groups C_1 and C_2, the scribe process has been performed from the rear side.

TABLE 2 Absolute mean improvements for the tunnel-oxide passivated contact (TOPCon) shingle cells by the passivated edge technology (PET) compared with their data directly after separation.

Group	Number new edges	$\Delta\eta$ ($\%_{abs}$)	ΔV_{OC} (mV)	ΔpFF ($\%_{abs}$)
C_1	1	0.31	1.6	1.0
	2	0.48	2.4	1.5
C_2	1	0.26	1.2	0.8
	2	0.37	1.4	1.2
C_3	1	0.28	1.3	0.8
	2	0.42	2.3	1.3

edge surfaces. As already found in the previous section, the metal contacts of the shingle cells are hardly affected by the applied thermal budgets from the Al_2O_3 layer deposition and the annealing step as the series resistances R_S are quite stable (not shown).

Cutting the host cells into shingle cells leads to lower initial losses for the outer shingle cells with only one new edge surface (C_X,1) compared with the inner shingle cells with two new edge surfaces (C_X,2). On average over the three groups C_1 to C_3, the larger performance drop for the inner shingle cells after separation is $\Delta\eta = -0.2\%_{abs}$, $\Delta V_{OC} = -2$ mV, and $\Delta pFF = -0.9\%_{abs}$.

The LSMC process in group C_1 leads to comparable efficient shingle cells as the LSMC process in group C_2. On the other hand, the TLS process in group C_3 is superior to both and yields more efficient shingle cells after separation by, in mean, $\Delta\eta = +0.15\%_{abs}$ (one new edge) and $\Delta\eta = +0.2\%_{abs}$ (two new edges). The advantage of the TLS can be explained by the microscope images of the newly created edge surfaces in Figure 7. The TLS for group C_3 leads to a very smooth surface across the entire cell thickness, whereas the LSMC process in group C_2 shows a scribe depth with a very rough surface of about half of the cell thickness. On the other hand, the LSMC process for group C_1 features a scribe depth of only around a third of the cell thickness.

After PET, a clear improvement is seen for all groups in Figure 6. Table 2 summarizes the respective mean gains for all shingle cells after PET compared with their data after separation. It is seen that the shingle cells with two new edge surfaces improve more by the PET in comparison with the shingle cells with just one new edge surface. This is a remarkable demonstration of the benefit provided by the PET. The shingle cells in group C_1, separated by LSMC, benefit the most from the PET ($\Delta\eta = +0.5\%_{abs}$ for "C_1,2") followed by group C_3, singulated by TLS ($\Delta\eta = +0.4\%_{abs}$ for "C_3,2"). But also, for the LSMC separation in group C_2, there is a clear improvement by the PET despite the partly very rough edge surface. The positive impact of the PET approach is therefore not limited to a certain separation process, as it shows a clearly efficiency-increasing effect in all cases.

It is remarkable that the PET leads to the fact that the *I*–*V* data difference in Figure 6B between the outer and inner shingle cells decreases in comparison with their larger difference directly after separation. The results suggest that the smoother the edge surface is, the lower is the difference between the outer and inner shingle cells after edge passivation by the PET approach: For C_3 and TLS (smoothest edge surface), the smallest *I*–*V* data difference is seen, whereas for C_2 and LSMC (roughest edge surface), the largest *I*–*V* data difference is seen.

The combination of TLS and PET in group C_3 yields the most efficient TOPCon shingle cells among the separation procedures examined. Applying TLS before PET allows for about $0.2\%_{abs}$ more efficient TOPCon shingle cells. The respective most efficient outer and inner shingle cells achieve $\eta = 21.92\%$ and $\eta = 21.88\%$, respectively. Both originate from the same host cell that has been initially tested to $\eta = 22.08\%$.

4 | SUMMARY AND CONCLUSION

This work demonstrates the fabrication of TOPCon shingle solar cells with low cutting-induced losses. The TOPCon shingle solar cells with a cell size of 26.46 mm × 158.75 mm are separated from full-square TOPCon host cells either by conventional LSMC from the rear side or by TLS from the front side with the boron emitter present. It is found that the TLS process optimized in this work yields up to $0.2\%_{abs}$ more

efficient shingle cells directly after separation in comparison with shingle cells that have been singulated by LSMC. It is shown that TLS can be performed such that no degradation of the surface passivation quality occurs in the vicinity to the dividing line. And thus, the increased surface recombination after TLS can be assigned solely to the newly created edge surfaces.

Likewise, it is demonstrated for the first time that the PET is also compatible with TOPCon shingle solar cell technology. In this work, the most efficient PET sequence consists of depositing an 8-nm-thin aluminum oxide (Al_2O_3) layer by thermal ALD at a temperature below 200°C in conjunction with subsequent hotplate annealing at 250°C. Stability measurements over a period of 11 months have shown a very stable passivation quality. Depending on the position the shingle cells were located within the host cell, the PET leads to improvements of varying magnitude. For "outer" shingle cells, that is, shingle cells that have been located far left or far right in the host cell, only one new edge surface is created during separation and an efficiency gain by PET of almost $0.3\%_{abs}$ is observed independent whether LSMC or TLS has been applied. For "inner" shingle cells that feature two new edge surfaces after separation, the gain by PET is larger and accounts to slightly more than $0.4\%_{abs}$ for LSMC and TLS. The positive and efficiency-increasing impact of the PET sequence is found to be not limited to a certain separation process applied.

The combination of TLS and PET reveals the most efficient TOPCon shingle cells within this work with an energy conversion efficiency of 22.0% for an inner shingle cell with two new and passivated edge surfaces. In comparison with LSMC-separated shingle cells after PET, the TLS technique yields about $0.2\%_{abs}$ more efficient shingle cells.

The investigations also reveal that both inner and outer shingle cells, which are separated by TLS and edge passivated by PET, achieve very similar efficiencies. This result is very valuable for subsequent string and module fabrication. It might allow that the shingle cells do not have to be sorted depending on their original position within the host cell, which would have a profitable effect on effort and costs.

ACKNOWLEDGEMENTS

The authors would like to thank all colleagues at Fraunhofer ISE and Solaria Corporation who supported the experiments within this work. This work was funded by Solaria Corporation and the German Federal Ministry for Economic Affairs and Climate Action within the research project "GutenMorgen" (contract number 03EE1101A). Open Access funding enabled and organized by Projekt DEAL.

DATA AVAILABILITY STATEMENT

Research data are not shared.

ORCID

Elmar Lohmüller https://orcid.org/0000-0001-6296-310X
Puzant Baliozian https://orcid.org/0000-0002-6679-1330
Leon Gutmann https://orcid.org/0000-0003-3426-1885
Leander Kniffki https://orcid.org/0000-0002-6962-815X
Armin Richter https://orcid.org/0000-0002-7232-8385
Lili Wang https://orcid.org/0000-0002-0417-4601
Ricky Dunbar https://orcid.org/0000-0003-0585-6011
Jonas D. Huyeng https://orcid.org/0000-0003-2735-8056
Ralf Preu https://orcid.org/0000-0003-1438-5303

REFERENCES

1. Stenzel F, Lee BG, Cieslak J, Schwabedissen A, Wissen D, Geißler S, Rudolph T, Faulwetter-Quandt B, Hönig R, Wasmer S, Bakowskie R, Buß D, Fertig F, Schaper M, Mette A, Müller JW. Exceeding 23% and mass production of p-Cz Q.ANTUM bifacial solar cells. In: *36th EU PVSEC*; 2019:96–99.
2. Baliozian P, Tepner S, Fischer M, Trube J, Herritsch S, Gensowski K, Clement F, Nold S, Preu R. The International Technology Roadmap for Photovoltaics and the significance of its decade-long projections. In: *37th EU PVSEC*; 2020:420–426.
3. Dickson DC. Photovoltaic semiconductor apparatus or the like. US patent: 2,938,938; 1956, 4998, 938, doi:10.1136/bmj.2.4998.938.
4. Glunz SW, Dicker J, Esterle M, Hermle M, Isenberg J, Kamerewerd FJ, Knobloch J, Kray D, Leimenstoll A, Lutz F, Osswald D, Preu R, Rein S, Schaffer E, Schetter C, Schmidhuber H, Schmidt H, Steuder M, Vorgrimler C, Willeke G. High-efficiency silicon solar cells for low-illumination applications. In: *29th IEEE*; 2002:450–453.
5. Tonini D, Cellere G, Bertazzo M, Fecchio A, Cerasti L, Galiazzo M. Shingling technology for cell interconnection: technological aspects and process integration. In: *33rd EU PVSEC*; 2017:38–41.
6. Baliozian P, Lohmüller E, Fellmeth T, Wöhrle N, Krieg A, Preu R. Bifacial p-type silicon shingle solar cells - the "pSPEER" concept. *Sol RRL*. 2018;3(2):1700171. doi:10.1002/solr.201700171
7. Baliozian P, Al-Akash M, Lohmüller E, et al. Postmetallization "passivated edge technology" for separated silicon solar cells. *IEEE J Photovolt*. 2020;10(2):390-397. doi:10.1109/JPHOTOV.2019.2959946
8. Zhu J, Roosloot N, Otnes G, Foss SE. Shingled solar module for BIPV application. In: *38th EU PVSEC*; 2021:765–768.
9. Gérenton F, Eymard J, Harrison S, Clerc R, Muñoz D. Analysis of edge losses on silicon heterojunction half solar cells. *Sol Energy Mater sol Cells*. 2020;204:110213. doi:10.1016/j.solmat.2019.110213
10. Harrison S, Bettinelli A, Portaluppi B, Giglia V, Carrière C, Sekkat A, Munoz-Rojas D, Barth V. Challenges for efficient integration of SHJ based solar cells in shingle module configuration. In: *37th EU PVSEC*; 2020:223–227.
11. Portaluppi B, Harrison S, Giglia V, Sekkat A, Munoz-Rojas D. Insights on cell edge defects impact and post-process repassivation for heterojunction. In: *37th EU PVSEC*; 2020:504–507.
12. Harrison S, Portaluppi B, Bertrand P, Giglia V, Martel B, Sekkat A, Munoz-Rojas D. Low temperature post-process repassivation for heterojunction cut-cells. In: *38th EU PVSEC*; 2021:167–171.
13. Nikitina V, Reinwand D, Fellmeth T, Mont SN, von Kutzleben D, Roessler T, Neuhaus H. Application of SHJ and TOPCon shingle cells in full-format and integrated solar modules. In: *8th WCPEC*; 2022.
14. ITRPV. International Technology Roadmap for Photovoltaic (ITRPV) - Results 2021; 2022.
15. Haschke J, Lemerle R, Aissa B, et al. Annealing of silicon heterojunction solar cells: interplay of solar cell and indium tin oxide properties. *IEEE J Photovoltaics*. 2019;9(5):1202-1207. doi:10.1109/JPHOTOV.2019.2924389
16. Luderer C, Messmer C, Hermle M, Bivour M. Transport losses at the TCO/a-Si:H/c-Si heterojunction: influence of different layers and annealing. *IEEE J Photovolt*. 2020;10(4):952-958. doi:10.1109/JPHOTOV.2020.2983989
17. Hermle M, Dicker J, Warta W, Glunz SW, Willeke G. Analysis of edge recombination for high-efficiency solar cells at low illumination densities. In: *3rd WCPEC*; 2003:1009–1012.

18. Wöhrle N, Fellmeth T, Lohmüller E, Baliozian P, Fell A, Preu R. The SPEER solar cell - Simulation study of shingled bifacial PERC-technology-based stripe cells. In: *33rd EU PVSEC*; 2017:844–848.
19. Zuehlke H-U, Eberhardt G, Mende P. TLS-dicing – the way to higher yield and throughput. In: *2008 International Symposium on Semiconductor Manufacturing (ISSM)*; 2008:301–304.
20. Eiternick S, Kaule F, Zühlke H-U, et al. High quality half-cell processing using thermal laser separation. *Energy Proced*. 2015;77:340-345. doi:10.1016/j.egypro.2015.07.048
21. Baliozian P, Münzer A, Lohmüller E, et al. Thermal laser separation of PERC and SHJ solar cells. *IEEE J Photovolt*. 2021;11(2):259-267. doi:10.1109/JPHOTOV.2020.3041251
22. Çetmeli M, Sekertekin B, Çaliskan M, Es F. Determination of effect of laser cutting method on the performance of bifacial PERC cells. In: *38th EU PVSEC*; 2021:242–245.
23. Münzer A, Baliozian P, Steinmetz A, et al. Post-separation processing for silicon heterojunction half solar cells with passivated edges. *IEEE J Photovolt*. 2021;11(6):1343-1349. doi:10.1109/JPHOTOV.2021.3099732
24. Guo J-H, Cotter JE, McIntosh KR, Fisher K, Chen FW, Karpour A. Edge passivation for small-area, high efficiency solar cells. In: *22nd EU PVSEC*; 2007:1348–1351.
25. Zhao J, Wang A, Altermatt PP, Zhang G. Peripheral loss reduction of high efficiency silicon solar cells by MOS gate passivation, by poly-Si filled grooves and by cell pattern design. *Prog Photovolt: Res Appl*. 2000;8(2):201-210. doi:10.1002/(SICI)1099-159X(200003/04)8:23.0.CO;2-V
26. Baliozian P, Klasen N, Wöhrle N, et al. PERC-based shingled solar cells and modules at Fraunhofer ISE. *Photovolt Int*. 2019;43:129-145.
27. Richter A, Benick J, Hermle M, Glunz SW. Excellent silicon surface passivation with 5 Å thin ALD Al_2O_3 layers: influence of different thermal post-deposition treatments. *Phys Status Solidi RRL*. 2011;5(5–6):202-204. doi:10.1002/pssr.201105188
28. Martel B, Albaric M, Harrison S, Dhainaut F, Desrues T. Addressing separation and edge passivation challenges for high efficiency shingle heterojunction solar cells. *Sol. Energy Mater. Sol. Cells*. 2023;250:112095. doi:10.1016/j.solmat.2022.112095
29. 3D-Micromac AG. microDICE - TLS-dicing™ system for separation of silicon and silicon carbide wafers. Available at: https://3d-micromac.com/laser-micromachining/laser-micromachining-systems/microdice/
30. Bassi N, Clerc C, Pelet Y, Hiller J, Fakhfouri V, Droz C, Despeisse M, Levrat J, Faes A, Bätzner D, Papet P. GridTOUCH: Innovative solution for accurate IV measurement of busbarless cells in production and laboratory environments. In: *29th EU PVSEC*; 2014:1180–1185.
31. Dingemans G, Terlinden NM, Pierreux D, Profijt HB, van de Sanden MCM, Kessels WMM. Influence of the oxidant on the chemical and field-effect passivation of Si by ALD Al_2O_3. *Electrochem Solid St*. 2011;14(1):H1-H4. doi:10.1149/1.3501970
32. Benton JL, Doherty CJ, Ferris SD, Flamm DL, Kimerling LC, Leamy HJ. Hydrogen passivation of point defects in silicon. *Appl Phys Lett*. 1980;36(8):670-671. doi:10.1063/1.91619

How to cite this article: Lohmüller E, Baliozian P, Gutmann L, et al. TOPCon shingle solar cells: Thermal laser separation and passivated edge technology. *Prog Photovolt Res Appl*. 2023; 31(7):729-737. doi:10.1002/pip.3680